Power Converter with a Galvanic Isolation and an Increased Efficiency

Dmitry Sorokin[1], Sergey Volskiy[2], Yury Skorokhod[1]
[1] Transconverter ltd, Russian Federation
[2] Moscow Aviation Institute (Technical University), Russian Federation

Corresponding author: Yury Skorokhod, skorohodu@yandex.ru
Speaker: Yury Skorokhod, skorohodu@yandex.ru

Abstract

The power converter for the SI310 FN4 test-bench is considered. It converts three-phase AC into six-phase AC with galvanic isolation. For such a converter, the parameters of a parallel twelfth-pulse rectifier with an input interphase and without an interphase transformer have been studied which less power losses. Expressions for the selection of diodes have been obtained. The total harmonic distortion of the input current is studied. The test results of the developed converter are presented. This article allows developers of power converters to make the right choice of the type of twelfth-pulse rectifier, and then select the type of diode.

1 Introduction

A power converter of type URN310 FN4 (URN), which has an input three-phase voltage of 400 V 50 Hz and an output six-phase voltage of 500 V, 50 Hz, is considered. It has a maximum output power of 310 kVA and regulated six-phase output voltage from 0 to 500 V.

Also, according to the technical requirements, the URN must have a galvanic isolation between the input and output voltage. Taking into account the maximum output voltage equals 500 V, we chose the DC link voltage equals 670 V.

URN is a part of the test-bench SI310 FN4, which is meant to test power converters of electric freight locomotives of 2(3)ES4K type.

To generate the DC link of URN voltage, we selected a power circuit that has an input isolating six-phase transformer with a frequency of 50 Hz and a twelfth-pulse rectifier (TPR). Such rectifiers have a number of advantages over circuits that use the conversion of electrical energy at an increased frequency [1]-[3]. Firstly, they have comparatively lower power losses in power semiconductor devices due to the conversion of electrical energy at a low frequency of 50 Hz. And most importantly, they have high reliability due to the small number of elements used (one input power transformer and 12 power diodes). The disadvantage of the selected scheme is the relatively large mass of the input power transformer, which has a frequency of 50 Hz. However, there was no restriction on the weight and measures of the URN in the technical requirements. Comparatively low power losses and high effectiveness were the main requirements when designing the power converter concerned.

The choice of using TPR is due to the following factors. Such rectifiers have small output voltage ripples, which allows the use of a relatively small LC output filter. Upon that, the TPR output voltage changes little from no load to rated load [4]-[7], which is the advantage of such a device.

Currently, series TPR, parallel TPR with an interphase transformer and parallel TPR without an interphase transformer are widely used.

The analysis [4]-[7] shows that the series TPR has almost 2 times larger current of the power diodes, which determines a relatively large power losses compared to the parallel TPR. On the other hand, the series TPR has half the maximum reverse voltage of the power diodes compared to the parallel TPR. Taking into account these circumstances, it is rational to use series TPR at an output voltage above 2000 V.

Due to the fact that we selected the DC link voltage equals to 670 V, we surveyed the use of parallel twelfth-pulse rectifiers with an interphase transformer (TPR1) and without an interphase transformer (TPR2).

2 Block Diagrams of a Power Converter

Fig. 1 shows a URN block diagram using TPR1, where TV1 is an input six–phase transformer; A1 and A2 units are three–phase bridge rectifiers that have output voltages $u_{R1}(t)$ and $u_{R2}(t)$; TV2 is an interphase transformer; A3 and A4 units are output three–phase

units; U_{DC1} is an output average voltage of TPR1, which forms the DC link voltage.

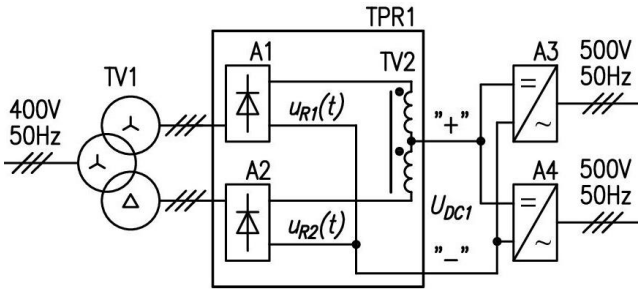

Fig. 1. The block diagram of the parallel TPR with an interphase transformer

In the block diagram shown in Fig. 1, the input three-phase voltage is connected to the primary three-phase windings (w_{A1}, w_{B1} and w_{C1}) of the input transformer TV1, which are connected by a "star". The first group of secondary three-phase windings (w_{A21}, w_{B21} and w_{C21}) is also connected by a "star", and the second group of secondary three-phase windings (w_{A22}, w_{B22} and w_{C22}) is connected by a "delta".

The secondary windings of the first and second groups of TV1 have transformation coefficients:

$$K_{TV21} = \frac{w_{A1}}{w_{A21}} = \frac{w_{B1}}{w_{B21}} = \frac{w_{A1}}{w_{A21}}; \quad (1)$$

$$K_{TV22} = \frac{w_{A1}}{w_{A22}} = \frac{w_{B1}}{w_{B22}} = \frac{w_{A1}}{w_{A22}}. \quad (2)$$

The windings of the input transformer TV1 have such a number of turns that the condition is fulfilled:

$$K_{TV22} = \sqrt{3}K_{TV21}. \quad (3)$$

The TV1 transformer, due to the secondary three-phase windings connected by "star" and "delta", forms two systems of three-phase output voltages shifted by 30 electrical degrees relative to each other. Thus, the TV1 transformer has a six-phase output voltage.

The voltages of the secondary three-phase windings of the input transformer TV1 are supplied to the inputs of the bridge three-phase rectifiers A1 and A2. The output voltages $u_{R1}(t)$ and $u_{R2}(t)$ of each rectifier A1 and A2 contain voltage ripples with a frequency of 300 Hz, which exceeds six times the frequency of 50 Hz of the electric line voltage. The output voltage $u_{R1}(t)$ of the first rectifier A1 has the same shape and amplitude as the output voltage $u_{R2}(t)$ of the second rectifier A2. At the same time, the output voltage $u_{R1}(t)$ of the first rectifier A1 is shifted relative to the output voltage $u_{R2}(t)$ of the second rectifier A2 by 30 electrical degrees due to the different connection of the secondary three-phase windings of the input transformer TV1.

The output voltages A1 and A2 through the interphase transformer TV2 are supplied to the input of the units A3 and A4. In this case the DC link voltage is defined from the expression:

$$u_{DC1}(t) = \frac{u_{R1}(t)+u_{R2}(t)}{2} \quad (4)$$

As a result, the output voltage ripples of TPR1 have an increased frequency of 600 Hz with a recurrence interval:

$$T_{TPR} = \frac{1}{12f}, \quad (5)$$

where f is the frequency of the input three-phase voltage of the URN.

In the recurrence interval from 0 to T_{TPR}, the output voltage TPR1 is calculated from the expression:

$$u_{out3} = \frac{\sqrt{2+\sqrt{3}}}{2} K_{TV1} U_{ain} \sin\left(\omega t + \frac{5\pi}{12}\right), \quad (6)$$

where K_{TV1} corresponds to K_{TV21} for TPR1; U_{ain} is the amplitude of the input line voltage URN; $\omega = 2\pi f$ is the angular frequency of the input voltage URN.

The A3 and A4 units are made according to a three-phase bridge circuit [1], [3]. Its converts the DC link voltage into a six-phase voltage with a frequency of 50 Hz and output voltage from 0 to 500 V.

Fig. 2 shows a block diagram of a URN using TPR2, which does not have an interphase transformer TV2, where U_{DC2} is the output average voltage of TPR2, which forms the DC link voltage.

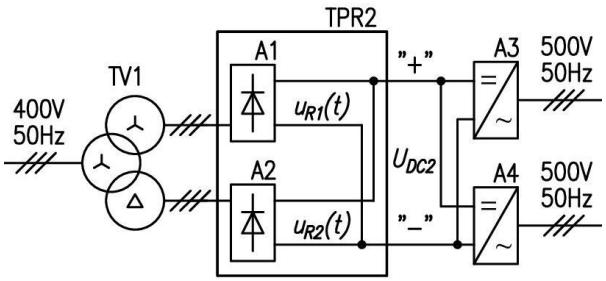

Fig. 2. The block diagram of the parallel TPR without an interphase transformer

The block diagram shown in Fig. 2 contains the same TV1 transformer as the block diagram shown in Fig. 1. In this regard, the TV1 also forms two systems of three-phase output voltages shifted by 30 electrical degrees relative to each other due to the secondary three-phase windings connected by "star" and "delta".

Similarly, the output voltages $u_{R1}(t)$ and $u_{R2}(t)$ of each rectifier A1 and A2 contain voltage ripples with a frequency of 300 Hz, which exceed six times the frequency of 50 Hz of the input line voltage of URN. In this case, the output voltage $u_{R1}(t)$ of the first rectifier A1 is shifted relative to the output voltage $u_{R2}(t)$ of the second rectifier A2 by 30 electrical degrees due to the different connection of the secondary three-phase windings of the transformer TV1.

Unlike TPR1, the output voltages A1 and A2 in TPR2 are connected in parallel without an interphase transformer. Unlike TPR1, the output voltages A1 and A2 in TPR2 are connected in parallel without an interfacial transformer TV2 directly to DC link. As a

result, in the recurrence interval from 0 to T_{TPR}, the output voltage TPR2 is calculated from the expression:

$$u_{DC2} = \begin{cases} K_{TV2}U_{ain}\sin\left(\omega t + \frac{\pi}{2}\right), 0 \le t < \frac{T_{TPR}}{2}; \\ K_{TV2}U_{ain}\sin\left(\omega t + \frac{\pi}{3}\right), \frac{T_{TPR}}{2} \le t < T_{TPR}, \end{cases} \quad (7)$$

where K_{TV2} corresponds to K_{TV21} for TPR2.

The ripples of the output voltage TPR2 and accordingly of the DC link voltage have an increased frequency of 600 Hz with a recurrence period of T_r, as in the TPR1.

The units A3 and A4 perform the similar functions as in the block diagram shown in Fig. 2.

3 Analysis of Parameters of Parallel Twelfth-Pulse Rectifiers

We assumed that TR1 and TR2 have the same output average voltages, which are equal to the DC link voltage:

$$U_{DC1} = U_{DC2} = U_{DC}. \quad (8)$$

In this case, the average output current of any TPR is defined as:

$$I_{TPR} = \frac{P}{\eta_A U_{DC}}, \quad (9)$$

where P is the URN output power; η_A are efficiency of the A3 and A4 units.

Taking into account (6)-(9), we investigated the following parameters of TPR1 and TPR2.

– duration (t_{on}) of the on-state of the power diode;

– the transformation coefficient (K_{TV21}), which provides the specified U_{DC};

– maximum repetitive instantaneous value (U_{MR}) of the power diode's reverse voltage;

– the average and effective value of the currents (I_{AV} and $I_{.RMS}$) of power diodes.

For clarity, we divided these parameters by the parameters of TPR1. The obtained relative parameters TPR1 and TPR2 are shown in Table I.

TABLE I. THE RELATIVE PARAMETERS OF THE TPR1 AND TPR2

TPR type	The parameter of TPR				
	t^*_{on}	K^*_{TV21}	U^*_{MR}	I^*_{AV}	$I^*_{.RMS}$
Parallel TPR with an interphase transformer	1	1	1	1	1
Parallel TPR without an interphase transformer	0.5	0.966	0.966	1	1.41

Table I shows that TPR2 has 3.4% less maximum repetitive instantaneous value of the power diode reverse voltage compared to TPR1. At the same time, due to the use of an interphase transformer, the effective current value of the TPR1 power diode is 41% less than the TPR2. This circumstance causes lower power losses in the power diodes in the TPR1 compared to the TPR2.

It is known that when rectifying a three-phase voltage with a frequency of 50 Hz, power diodes have low switching losses that can be ignored. In this regard, we surveyed the junction temperature depending only on the power of conduction losses in the power diodes of the considered TPR1 and TPR2.

The conduction power losses in the diode consists of the power losses $P_{VD.V}$ at the threshold voltage $V_{(T0)}$ and the power losses $P_{VD.r}$ at the active resistance r_T [3], [9], [10]:

$$P_{VD.V} = \frac{1}{T}\int_0^T i_{VD}(t)V_{(T0)}dt; \quad (10)$$

$$P_{VD.r} = \frac{1}{T}\int_0^T i_{VD}(t)^2 r_T dt, \quad (11)$$

where $i_{VD}(t)$ is the current of the power diode; T is the period of the input voltage.

The results of the calculation of conduction power losses in power diodes are shown in Table II.

TABLE II. THE CONDUCTION POWER LOSSES IN DIODES

TPR type	The conduction power losses		
	$P_{VD.V}$	$P_{VD.r}$	$P_{VD.V} + P_{VD.r}$
Parallel TPR with an interphase transformer	$\frac{I_{TPR}V_{(T0)}}{6}$	$\frac{I^2_{TPR}r_T}{6}$	$\frac{I_{TPR}V_{(T0)}}{6} + \frac{I^2_{TPR}r_T}{6}$
Parallel TPR without an interphase transformer	$\frac{I_{TPR}V_{(T0)}}{6}$	$\frac{I^2_{TPR}r_T}{12}$	$\frac{I_{TPR}V_{(T0)}}{6} + \frac{I^2_{TPR}r_T}{12}$

Table II shows that the use of the interphase transformer TV2 does not lead to a decrease in the power losses $P_{VD.V}$ compared to TPR2. Upon that, TPR1 has two times less power losses $P_{VD.r}$, which are associated with the active resistance r_T of power diodes in the on-state. This is due to the fact that the effective current value of the power diode TPR1 is 41% less than TPR 2. Thus, TPR1 has the lowest power losses in the power diodes.

Each TPR of URN has two heatsink on which six power diodes of A1 and A2 are installed. We assumed that each TPR power diode has the same thermal resistances junction-substrate (R_{j-c}), substrate-case (R_{c-s}) and case-ambient (R_s). Taking into account the accepted assumptions, each power diode of the considered TPR has a simple single-line thermal model [1], [11], [12]. Therefore, the temperatures T_{j1} and T_{j2} of the power diode junction of TPR1 and TPR2 are calculated as:

$$T_j = T_e + (P_{VD.TO} + P_{VD.r})R_{\Sigma th}, \quad (12)$$

where $R_{\Sigma th} = R_{j-c} + R_{c-s} + R_s$.

Taking into account the data in Table II, we obtained an expression for calculating the temperature T_{j1} and T_{j2} of a power diode junction in TPR1 and TPR2 depending on the average output current I_{TPR}:

$$T_{j1} = T_e + (\frac{I_{TPR}V_{(T0)}}{6} + \frac{I_{TPR}^2 r_T}{12})R_{\Sigma th}; \quad (13)$$

$$T_{j2} = T_e + (\frac{I_{TPR}V_{(T0)}}{6} + \frac{I_{TPR}^2 r_T}{6})R_{\Sigma th}. \quad (14)$$

From (13) and (14) we have obtained expressions for calculating the average output current I_{TPR1} и I_{TPR2} of the TPR1 and TPR2 at a given temperature T_{jg} of a power diode junction:

$$I_{TPR1} = -\frac{V_{(T0)}}{2r_T} + \sqrt{\left(\frac{V_{(T0)}}{2r_T}\right)^2 + 6\frac{T_{jg}-T_e}{R_{\Sigma th}r_T}}; \quad (15)$$

$$I_{TPR2} = -\frac{V_{(T0)}}{r_T} + \sqrt{\left(\frac{V_{(T0)}}{r_T}\right)^2 + 12\frac{T_{jg}-T_e}{R_{\Sigma th}r_T}}. \quad (16)$$

Then, we have obtained expressions for calculating the average current $I_{VD.AV1}$ и $I_{VD.AV2}$ of a power diode of the TPR1 and TPR2 at a given temperature T_{jg} of a power diode junction:

$$I_{VD.AV1} = -\frac{V_{(T0)}}{12r_T} + \sqrt{\left(\frac{V_{(T0)}}{12r_T}\right)^2 + \frac{T_{jg}-T_e}{6R_{\Sigma th}r_T}}; \quad (17)$$

$$I_{VD.AV2} = -\frac{V_{(T0)}}{6r_T} + \sqrt{\left(\frac{V_{(T0)}}{6r_T}\right)^2 + \frac{T_{jg}-T_e}{3R_{\Sigma th}r_T}}. \quad (18)$$

We introduced an overcurrent coefficient equals to the ratio of the calculated maximum average current $I_{mAV.i}$ of the TPR power diode, obtained from (17) and (18) taking into account the maximum permissible temperature $T_{j.max}$ of the power diode junction, to the permissible average value of the selected power diode current $I_{AV.n}$:

$$K_{ov.i} = \frac{I_{mAV.i}}{I_{AV.n}}, \quad (19)$$

where the index i (1 or 2) corresponds to the TPR1 or TPR2 type number; the index n corresponds to the selected power diode number.

We calculated the overload coefficients $K_{ov.1}$ and $K_{ov.2}$ for TPR1 and TPR2 in relation to the selected power diodes SKKD81, SKKD100 и SKKD162 at the maximum permissible temperature $T_{j.max}$, equals to 125°C. The calculation results are shown in Table III.

TABLE III. RESULTS OF CALCULATING THE OVERLOAD FACTOR

Diode type	The parameter						
	$V_{(T0)}$, V	r_T, mOhm	$R_{\Sigma th}$, K/W	$T_{j.max}$, °C	$K_{ov.1}$	$K_{ov.2}$	$\frac{K_{ov.2}}{K_{ov.1}}$
SKKD81	0.85	1.8	1.03	125	0.85	1.03	1.22
SKKD100	0.85	1.3	0.98	125	0.97	1.16	1.20
SKKD162	0.85	1.2	0.51	135	1.32	1.61	1.22

Comparison of the obtained values of the coefficients $K_{ov.1}$ and $K_{ov.2}$ allows to conclude that TPR1 can have about 20% more output average current, at which the junction temperatures of power diodes reach $T_{j.max}$, compared with TPR2.

Electrical and thermal simulation models of the considered TPR were developed using MATLAB Simulink [13], [14]. The accepted assumptions were taken into account in the computer thermal model. Computer simulation confirmed the accuracy of the analytical expressions obtained.

Taking into account the conducted research, we decided to use TPR1 in URN according to the block-diagram in Fig. 1. This is due to the fact that TPR1 has lower power losses in power diodes and, as a result, a lower operating temperature of junctions of power diode compared to TPR2.

4 Study of Total Harmonic Distortion of the Input Current

By means of the developed simulation model, we studied the total harmonic distortion (*THD*) of the input current URN using TPR1. When calculating *THD*, the harmonics of the input current were taken into account, including a harmonic with a frequency of 2500 Hz.

Obviously, the shape of the phase current URN with TPR1 depends on the inductance of the input circuit (L_{in}), the leakage inductance (L_{s1}) of the TV1 and the leakage inductance (L_{s2}) of the TV2.

We researched the dependence of the harmonic coefficient *THD* of the input current of the considered URN if an additional inductance L_f is installed between the TPR1 and DC link. In order to exclude the influence of the inductances of the input circuit on the harmonic coefficient *THD*, it was assumed that $L_{in} = L_{s1} = 0$.

The simulation results showed that *THD* varies from 13.3 to 14.1% when the L_f changes from 0 to ∞. Thus, *THD* does not depend much on the additional inductance L_f. Accordingly, the leakage inductance L_{s2} of the TV2 also has almost no effect on *THD*.

In the process of computer simulation, we found out that units A1 and A2 have different output currents, if the power diodes of these units have different parameters ($V_{(T0)}$ and r_T), the windings of the TV1 and TV2 have different active resistances. In this regard, these units A1 and A2 have different output powers P_{A1} and P_{A2}. It has been investigated how different output powers of P_{A1} and P_{A2} affect *THD*. We assumed that $P_{A1} \le P_{A2}$, and introduced the symmetry coefficient:

$$\chi = \frac{P_{A1}}{P_{A2}}. \quad (20)$$

Computer simulation showed that even when changing χ from 1 to 0, the additional inductance L_f and the leakage inductance L_{s2} of the TV2 have almost no affect to *THD*. Also, we studied how *THD* depends on the total inductance $L_\Sigma = L_{in} + L_{s1}$ and the coefficient χ.

Fig. 3 shows the results of computer simulation, where the solid line corresponds to $\chi = 1$; the dashed line corresponds to $\chi = 0.8$; the line with asterisks corresponds to $\chi = 0.6$.

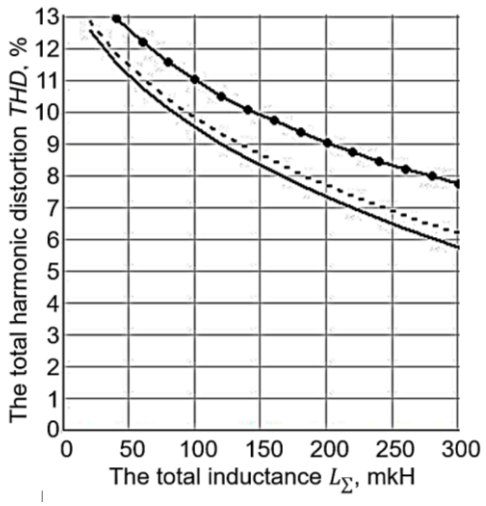

Fig. 3. The dependence of total harmonic distortion

Fig. 3 shows that *THD* increases with decreasing L_{Σ} and χ. According to [15], the permissible *THD* for prolonged exposure should be no more than 8% and for short-term exposure should be no more than 11%. In order to provide the required *THD*, it is necessary that $L_{\Sigma} = 160$ μH at $\chi = 1$, $L_{\Sigma} = 177$ μH at $\chi = 0.8$ and $L_{\Sigma} = 277$ μH at $\chi = 0{,}6$. To determine the additional input phase inductance L_{ad}, which will provide the required *THD* equals to 8%, the following algorithm is proposed. The parameters L_{s1} and χ of the developed URN is defined. Using the developed simulation model, L_{Σ} is calculated for the obtained parameters L_{s1} and χ. Then the required value of the additional input phase inductance is determined:

$$L_{ad} = L_{\Sigma} - L_{s1}. \qquad (21)$$

The proposed algorithm allows, by means of the given parameters L_{s1} and χ using computer simulation and (21), to determine an additional input phase inductance at which the considered URN with TPR1 has an acceptable *THD* (for example, no more than 8%).

5 Test Results

The developed URN is shown in Fig. 4. According to the block diagram Fig. 1, it contains an external input transformer TV1, which converts an input three-phase line voltage of 400 V, 50 Hz to a six-phase voltage of 500 V, 50 Hz. Then the units A1 and A2 rectify the obtained six-phase voltage. As a result, a DC link 670 V is generated at the output of the interphase transformer TV2, which units A3 and A4 convert to a six-phase voltage regulable from 0 to 450 V.

The developed URN is a part of the SI310 FN4 test-bench, which is meant to test PSN235 N2 converters. Such power converters are used on electric freight locomotives of type 2(3)ES4K.

The power diodes of each A1 and A2 unit are set up in a separate heatsink, which has three built-in cooling fans.

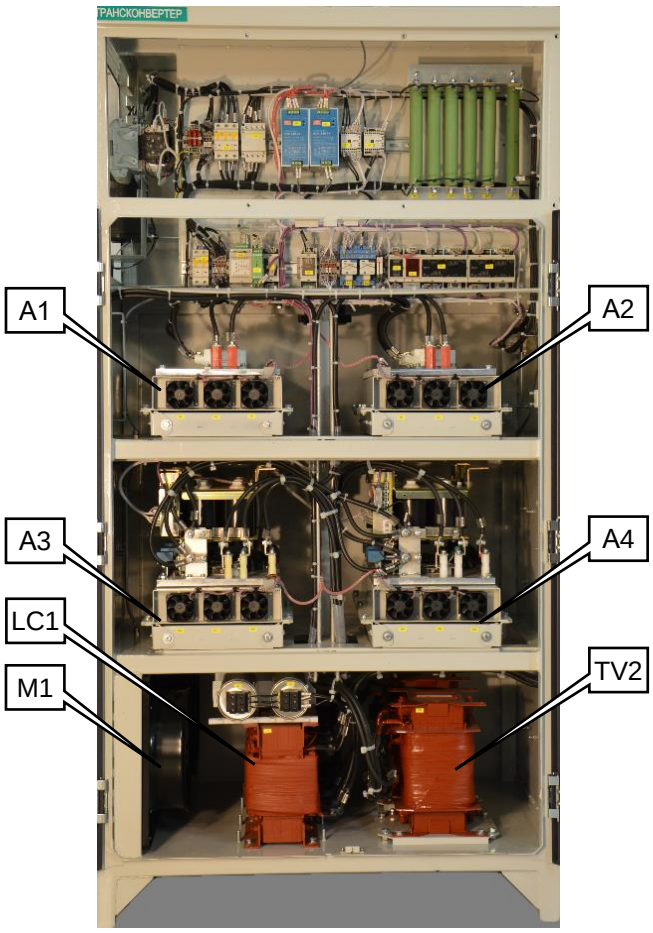

Fig. 4. The developed URN

The power transistors of each A3 and A4 unit are also set up in a separate heatsink, which also have three built-in cooling fans. Sine filters LC1 and LC2 are installed at the output of each A3 and A4 unit, which convert the PWM voltages of A3 and A4 units into sinusoidal voltages. The sine filter LC2 is installed behind the sine filter LC1. The fan M1 provides forced air cooling of the sine filters LC1, LC2 and the interphase transformer TV2. The developed URN has the maximum peak power, equals to 310 kVA and the symmetry coefficient $\chi = 0.87$.

Fig. 5 shows oscillograms of the input phase current (1) of the developed URN and of the input phase current (2) of the A1 unit. According to the obtained oscillograms, *THD* is equal to 9.57%, which corresponds to $L_{\Sigma f} = 105$ μH. To achieve *THD* equal to 8%, we must have $L_{\Sigma\,8\%}$ equal to 167 μH.

The additional input phase inductance is determined from the expression:

$$L_{ad} = L_{\Sigma\,8\%} - L_{\Sigma f} = 167 - 105 = 62 \qquad (21)$$

Thus, an input phase inductance L_{ad} of 62 μH must be added to the URN in order for *THD* to comply with the requirements [15].

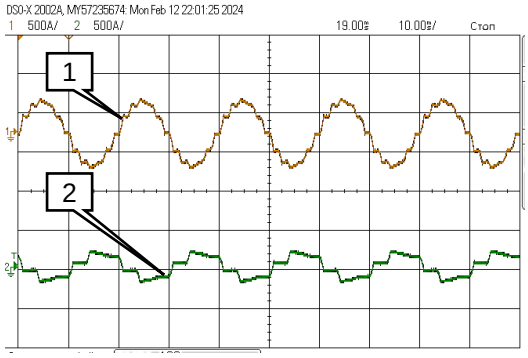

Fig. 5. Oscillograms of the currents

6 Conclusion

1 Due to the use of an interphase transformer, the effective current value of the TPR1 power diode is 41% less compared to TPR2. This circumstance causes lower power losses in the power diodes in TPR1 compared to TPR2.

2 A parallel twelfth-pulse rectifier with an interphase transformer can have about 20% greater output average current, at which the junction temperatures of the diodes reach a maximum value compared to TPR2.

3 Computer simulation of the using MATLAB Simulink confirmed the correctness of the results obtained.

4 The leakage inductance of the interphase transformer has almost no effect on *THD*.

5 *THD* increases with a decrease in the total input inductance and an increase in the difference between the parameters of the power diodes and the active resistances of the windings of the input transformer and of the interphase transformer.

6 An algorithm for calculating the additional input phase inductance, at which the considered URN has the required *THD* is proposed.

7 The obtained results allow electrical engineers to select both the type of twelfth-pulse rectifiers and the type of power diode for the selected rectifier and the parameters of the additional input inductance.

7 References

[1] G. C. Zinoviev: Power Electronics, Moscow, Russian Federation, Yurayt, 2015.

[2] N. Volskiy and M. Krapivnoi: Development of a Power Transformer for Fast Charging Station, Proc. ICEEE-23, Istanbul, Turkey, 2023, 375-380.

[3] V. Meleshin: Transistor Converter Technology, Moscow, Russian Federation, Technosphere, 2006.

[4] F. Meng, T. Jiang and L. Gao: A Series-Connected 12-Pulse Rectifier Based on Power Electronic Phase-Shifting Transformer, Proc. ICEMS-2019, Harbin, China, 2019, 1-5, doi: 10.1109/ICEMS.2019.8921470.

[5] G. Su, Y. Li, S. Liu, X. Wang: Optimized Design for the 12-Pulse Uncontrolled Rectifier with a Coupling Interphase Reactor, Proc. ICIBA-2020, Chongqing, China, 2020, 1300-1304.

[6] B. Wu, M. Narimani: High-Power Converters and AC Drives, 2nd Edition, Wiley-IEEE Press, 2017.

[7] P. Bisoi, S. C. Swain: Optimized Operation of Interphase Transformer for Power Converters Operating in Parallel and Its Analytical Characterisation, International Journal of Engineering Research & Technology, Bangalore, India, vol. 03, issue 12, 2014, 957-960.

[9] L. A. Bessonov, V. L. Bessonov: Theoretical Foundations of Electrical Engineering. Electric Circuits, Moscow, Russian Federation, Yurayt, 2019.

[10] F. Wang, Z. Zhang, R. Chen: Design of Three-Phase AC Power Electronics Converters, Wiley-IEEE Press, 2023.

[11] E. P. Safonov, V. Y. Frolov and E. D. Paramonov: Semiconductor Diode Model with Thermal Behavior for a DC Current Limiting Device, Proc. Seminar on EEACS2023, Saint Petersburg, Russian Federation, 2023, 267-270.

[12] L. Montaner, A. Kaïd, F. Roqueta, L. Hébrard and J. -B. Kammerer: Discrete Packaged Power Diode's Electro-Thermal Behaviour Modelling Method in a Standard CAD Environment, THERMINIC-23, Budapest, Romania, 2023, 1-5, doi: 10.1109/THERMINIC60375.2023.10325886.

[13] S. German-Galkin: Virtual Laboratories of Semiconductor Systems in Matlab-Simulink Environment + CD: Textbook.1st ed, St. Petersburg, Russian Federation, Lan, 2021.

[14] V. P. Dyakonov: Simulink. Self-instruction, Moscow, Russian Federation, DMK-press, 2015.

[15] GOST IEC/TR 61000-3-14-2019, Electromagnetic compatibility (EMC). Part 3-14. Assessment of Emission Limits of Harmonic, Interharmonic, Voltage Fluctuation and Unbalance for the Connection of Disturbing Installations to LV Power Systems, Moscow, Russian Federation, 2019.